Towards 3-D Multi-scale Adjoint Waveform Tomography of the Lithosphere and Underlying Mantle Beneath Southeast Asia

Deborah Wehner[1], Nienke Blom[1], Nick Rawlinson[1], Meghan Miller[2], Sri Widiyantoro[3], Daryono[4]

[1] University of Cambridge (United Kingdom) [2] Australian National University, Canberra (Australia)

[3] Institut Teknologi Bandung (Indonesia) [4] Meteorology, Climatology and Geophysical Agency (Indonesia)

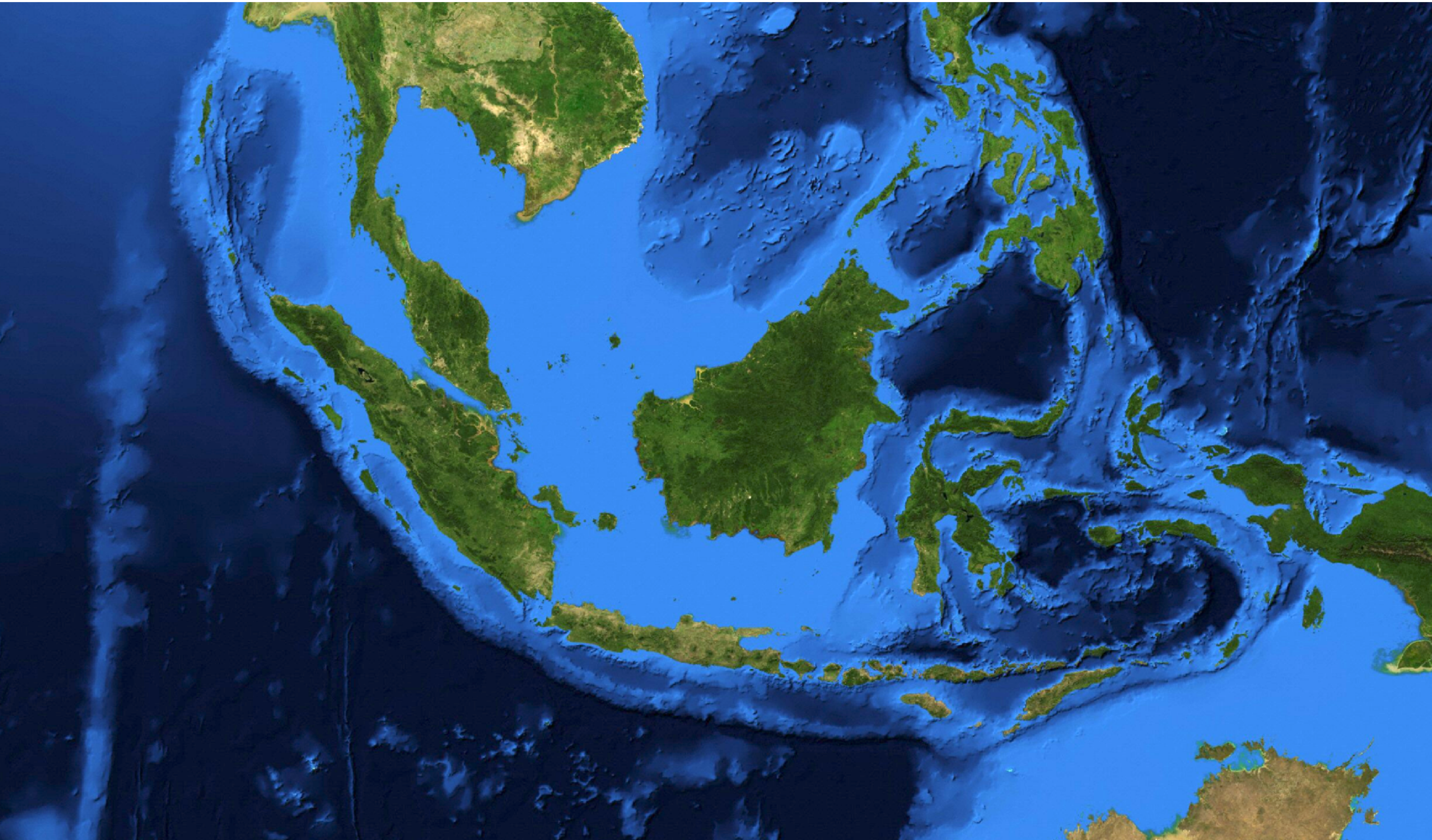

Motivation

The aim of this project is to obtain a **3-D seismic structural model of lithosphere and underlying mantle** beneath Southeast Asia.

Southeast Asia is one of the **most complex tectonic regions on Earth** and known to be vulnerable to natural hazards as evidenced by frequent large earthquakes and volcanic eruptions (e.g. Sumatra earthquake in 2004, Krakatoa eruption in 2018).

Adjoint waveform tomography is especially suitable for imaging such complex regions since it can account for the effects of anisotropy, anelasticity, wavefront healing, interference and (de)focusing that can hamper other seismological methods.

Mt Kinabalu, Malaysia

In a nutshell: Southeast Asian waveform tomography

We present a continental-scale 3-D seismic structural model of the upper mantle beneath Southeast Asia for periods down to 40 s using adjoint waveform tomography
[often referred to as *full-waveform inversion*]

The inversion parameters are restricted to
- isotropic P wave velocity (v_P)
- radially anisotropic S wave velocity (v_{SH} , v_{SV})
- density

We are imaging subsurface structures down to the mantle transition zone, including multiple subduction zones

Our model reveals strong heterogeneities > 12 %
[strongest variation for v_{SH} parameter]

200 km depth slice

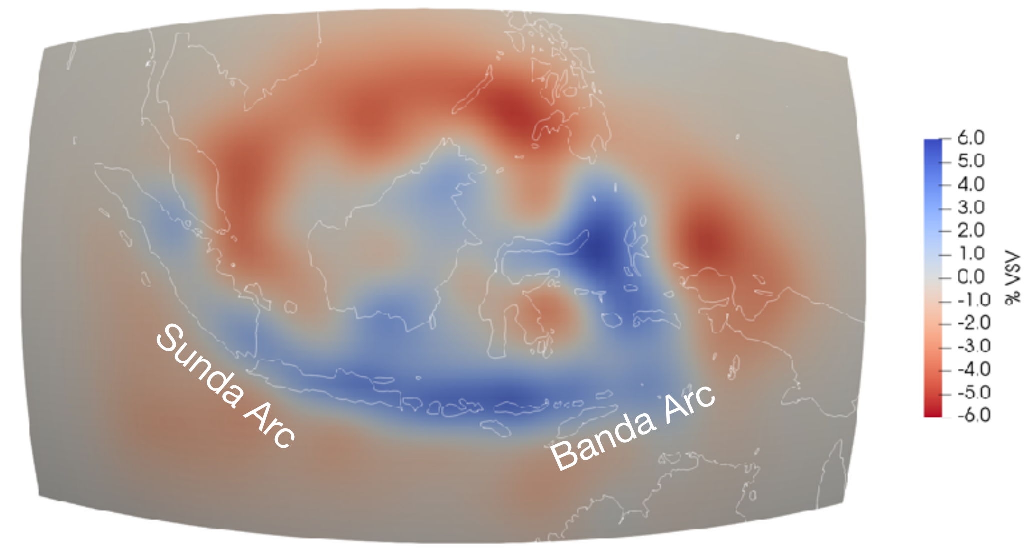

cross-section

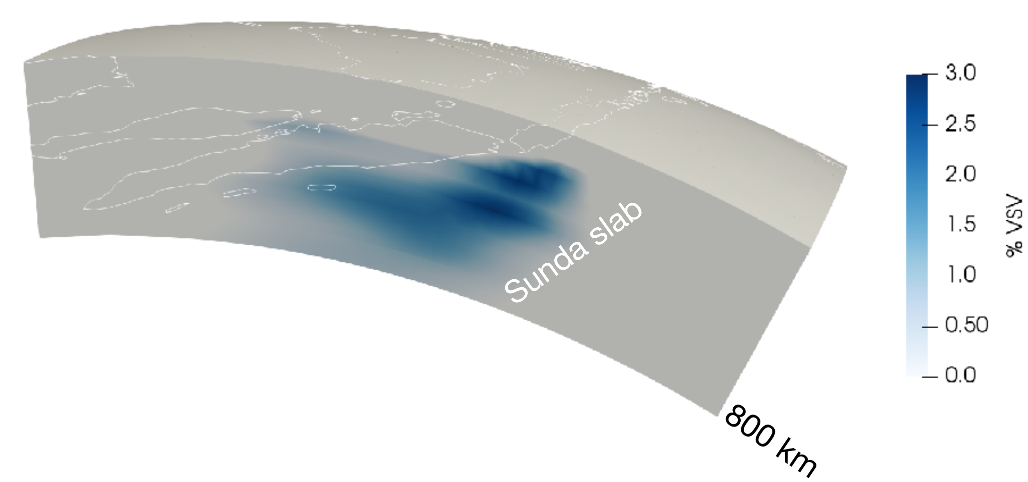

v_{SV} depth slice and cross-section revealing the Sunda slab

Tectonic setting of Southeast Asia

- Southeast Asia is one of the most **tectonically complex** parts of the Earth
  [it is located within the triple junction of the Australian, Eurasian and Philippine Sea plates]
- The region provides a unique laboratory to investigate **ongoing subduction as well as post-subduction settings** [e.g. Hall, 2012; Zenonos et al, 2019]
- Large-magnitude earthquakes along the Sunda trench represent a significant natural hazard (e.g. the 2004 Sumatra earthquake); The East is characterised by several minor tectonic plates and deep earthquakes

Seismicity M_w > 5.5 (2000-2019)
[circle size proportional to magnitude]

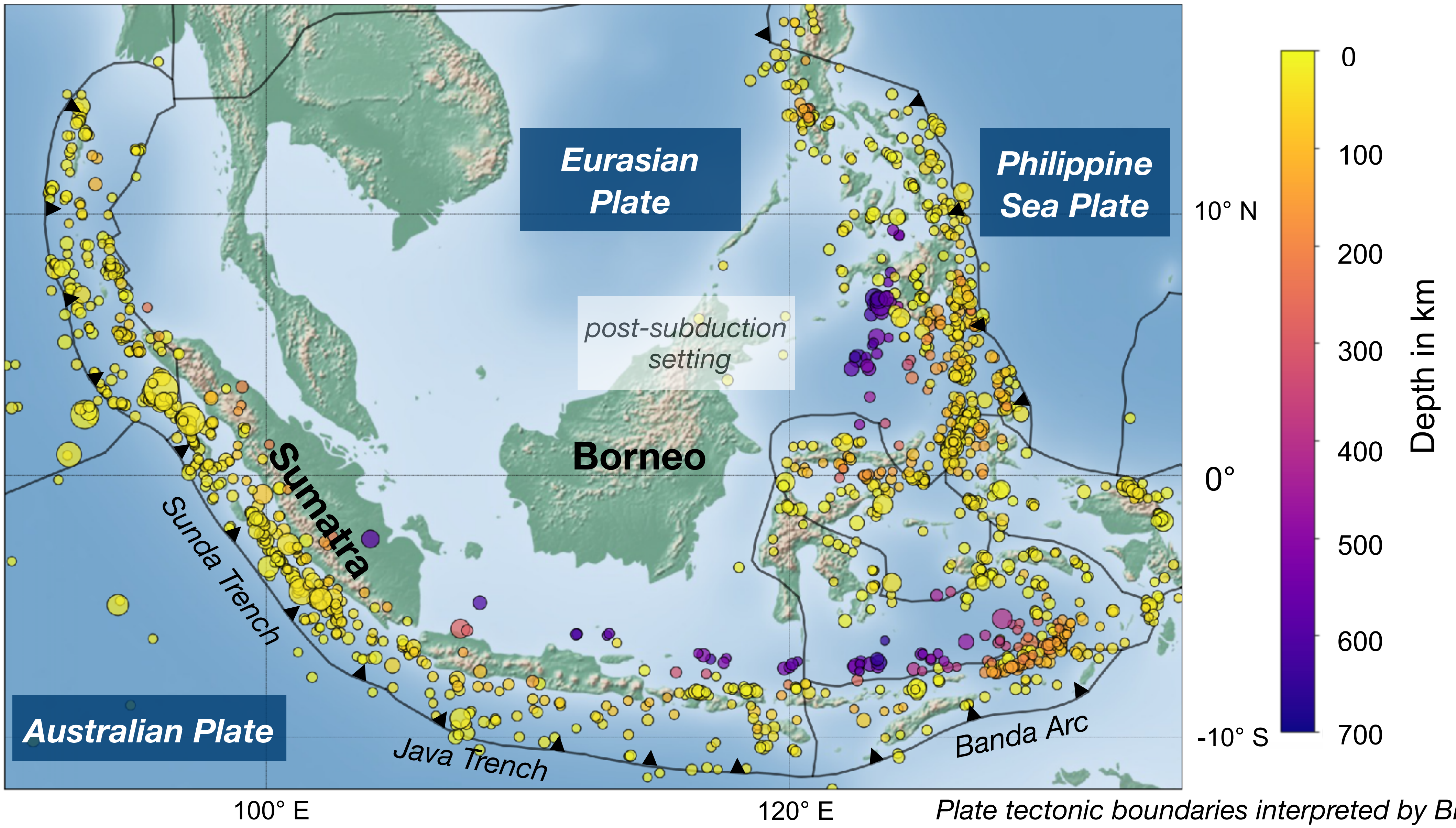

Plate tectonic boundaries interpreted by Bird (2003)

Data availability

There are **few public stations** ▽ available within the area
[mainly targeting hazardous regions]

However, our recently deployed networks of broadband seismometers ▼ as well as access to restricted networks ▼ promise a significant improvement in data coverage

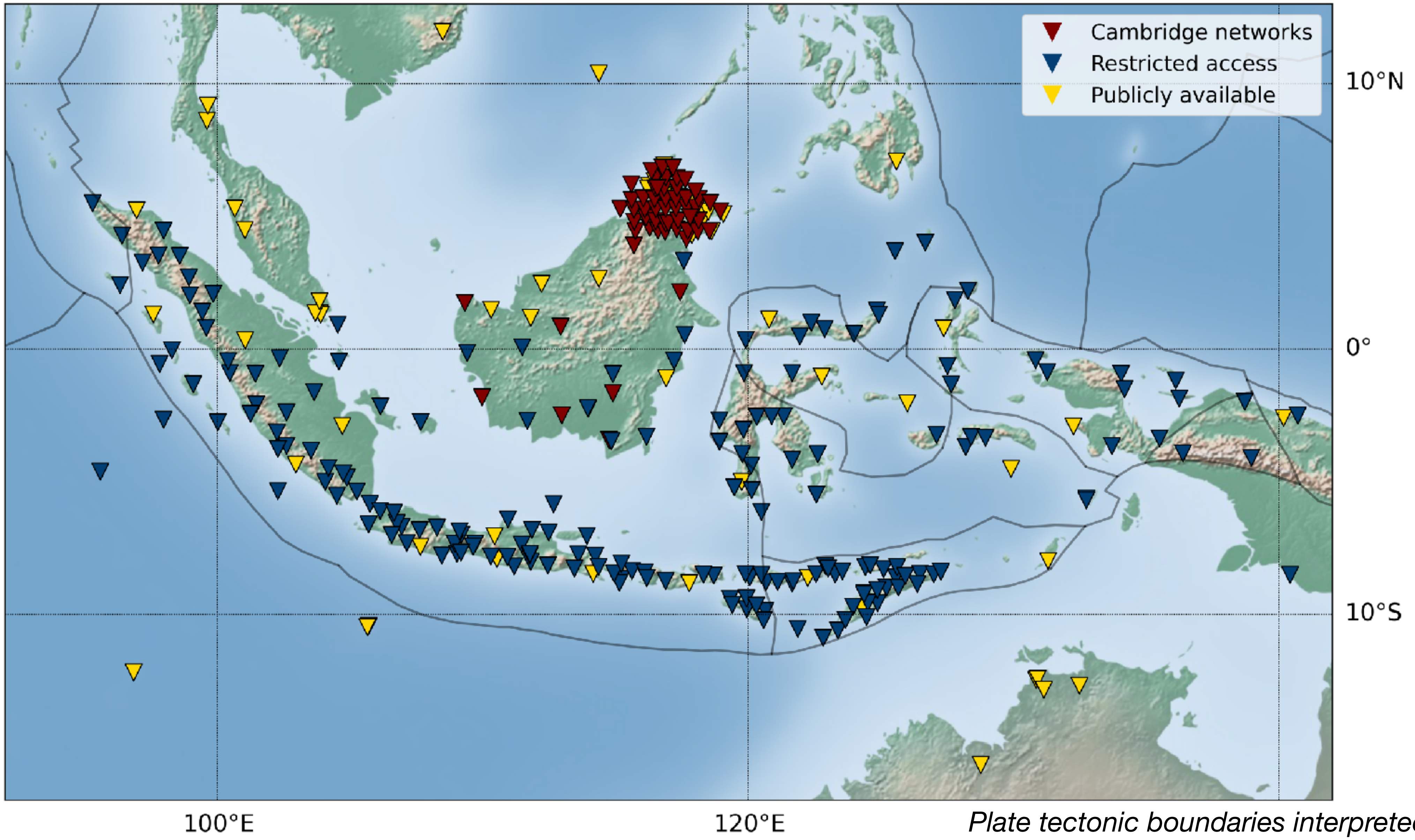

Plate tectonic boundaries interpreted by Bird (2003)

Adjoint waveform tomography

For complex regions, such as Southeast Asia, adjoint waveform tomography is an especially suitable imaging method since it can account for **the effects of anisotropy, anelasticity, wavefront healing and interference**.

However, the method is computationally expensive as it employs the computation of the **3-D seismic wave field**
[visualised on the right]

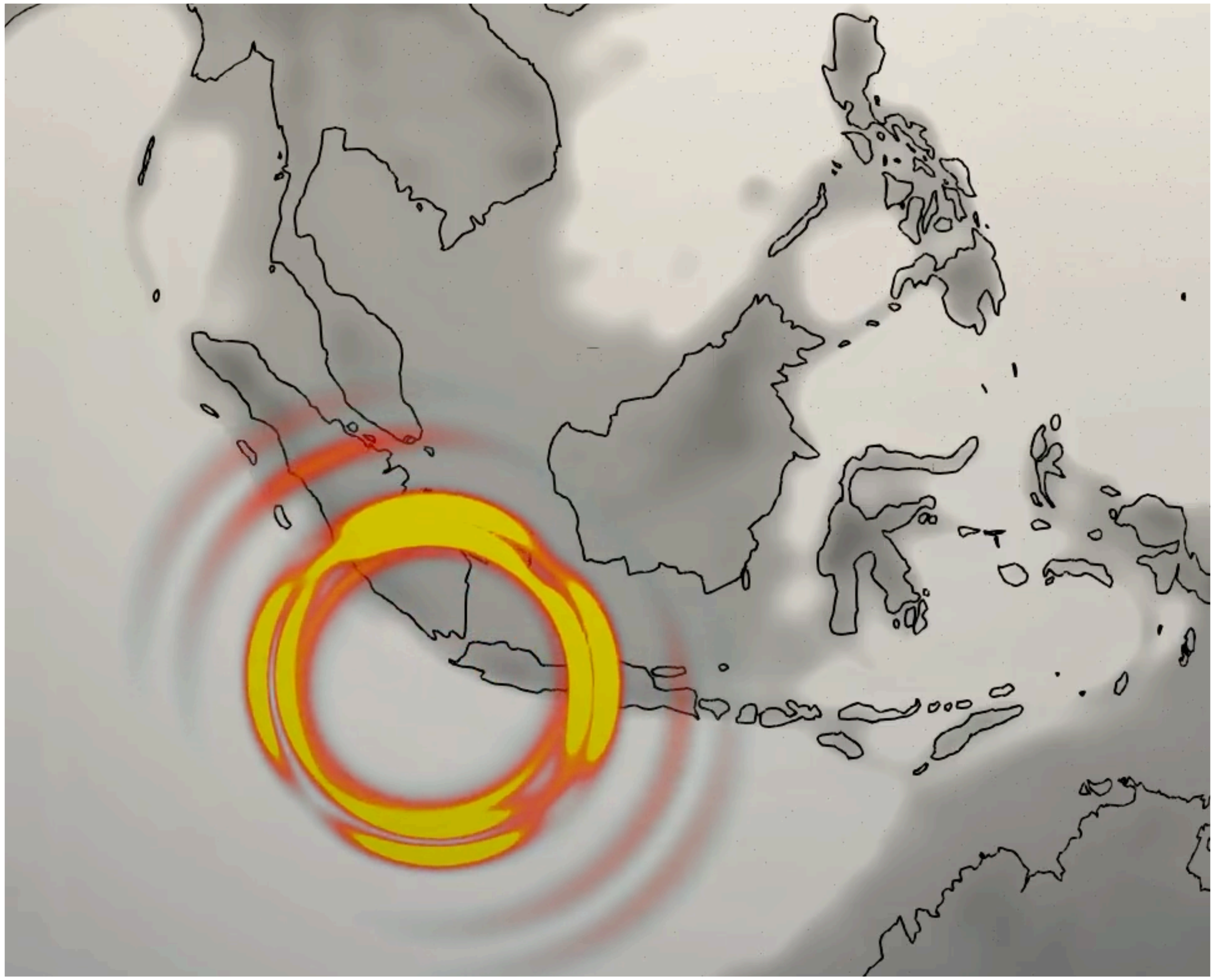

M_w 6.9 earthquake on 2 August 2019
(filtered from 30 to 150 s)

Adjoint waveform tomography

Adjoint waveform tomography is an **inverse problem** where an initial model is updated based on the difference between synthetics and observed waveforms.

(1) Synthetic seismograms are computed by **simulating the 3-D wavefield**, thereby taking into account both body and surface waves.

(2) Synthetic and observed waveforms are compared using a **suitable misfit measure.**
[this defines the measurement(s) made on a seismogram]

(3) A **misfit gradient is computed** using adjoint techniques through the construction of **sensitivity kernels.**

(4) The current model is updated using a **gradient-based optimisation scheme** (e.g. L-BFGS).

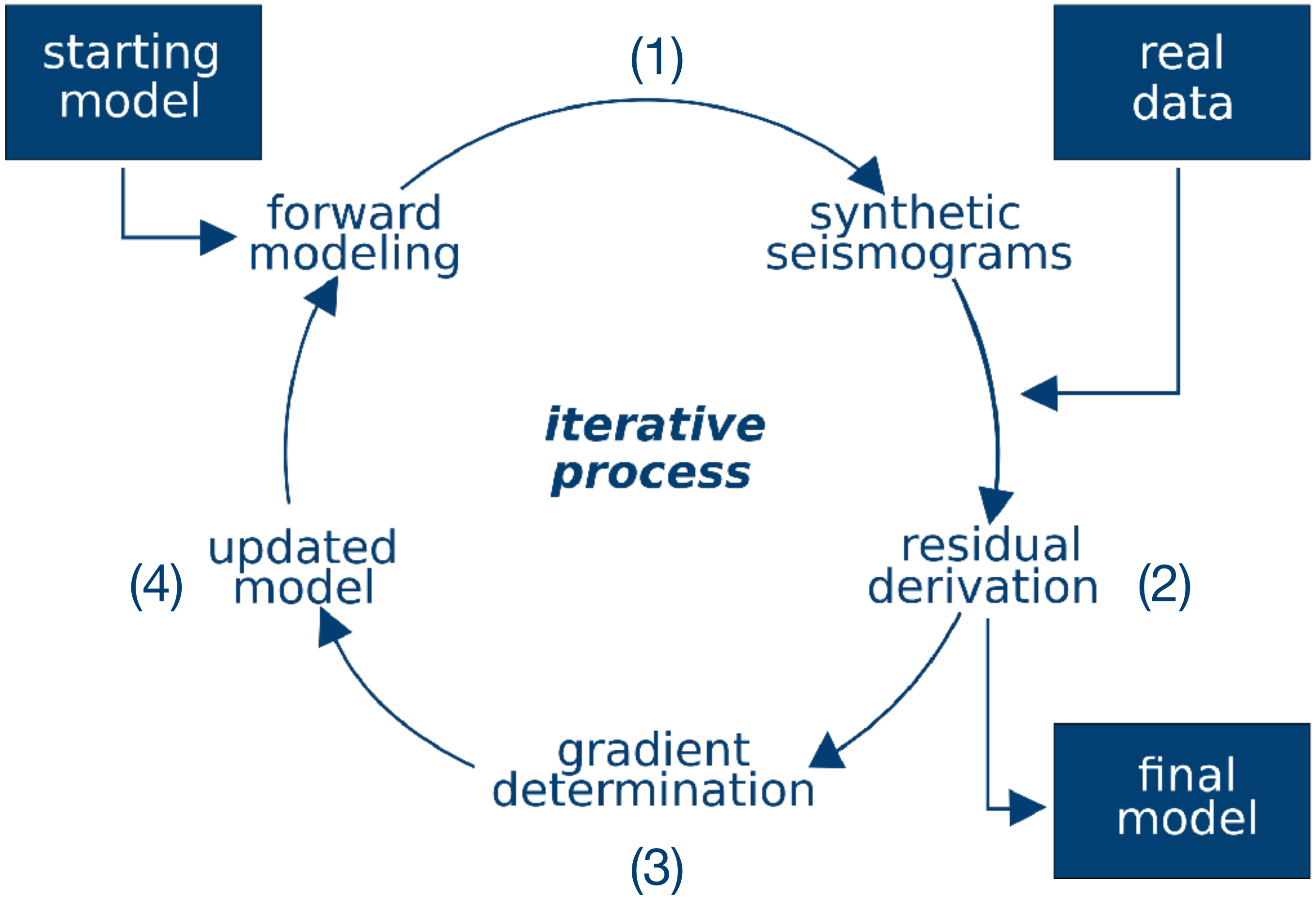

Southeast Asian waveform tomography

Our initial model is taken from the *Collaborative Seismic Earth Model* (Fichtner et al., 2018)
[for this study area, this is a modified version of the one-dimensional anisotropic *PREM* (Dziewonski & Anderson, 1981)]

The event catalogue (see figure below) contains up to **118 events (M_w5.3 - 7.5)** per period band
[moment tensors are retrieved from the *GCMT catalogue*, Ekström et al., 2012;
source times functions are reviewed using *SCARDEC,* Vallée et al., 2011]

Further, we implement a **geographical station weighting** as proposed by Ruan et al. (2019)
[to balance the effect of a heterogeneous station coverage]

Mesh extension:
~5,000 x 3,500 x 800 km
[plus absorbing boundaries
to avoid artificial reflections]

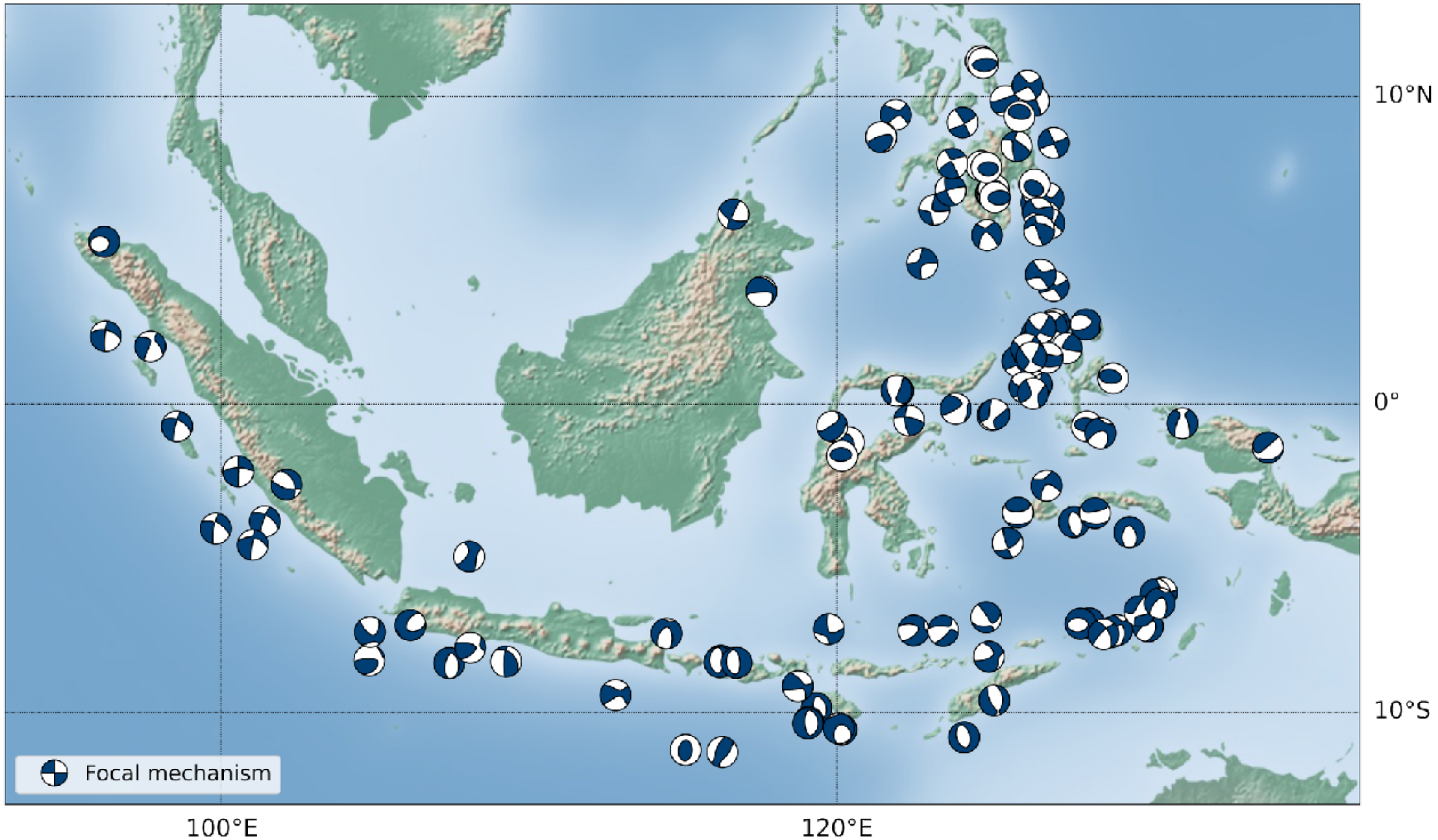

Southeast Asian waveform tomography

Realistic synthetics are obtained using *Salvus* (Afanasiev et al., 2019), accounting for **anisotropy, attenuation, topography and bathymetry**

Windows define the part of a seismogram we are making measurements on. This is necessary to avoid noisy data and cycle skips [windows are suggested by *FLEXWIN,* Maggi et al., 2009]

Most objective functions favour large-amplitude signals. In particular **depth information**, derived mostly from small-amplitude body waves, ends up being lost. We maximise sensitivity to deep structure by **separating small-amplitude body waves from large-amplitude surface waves** as shown below

The waveform difference is quantified using a **time-frequency misfit** as proposed by Fichtner et al. (2008) [which is based on a time-frequency transform of both observed data and synthetics]

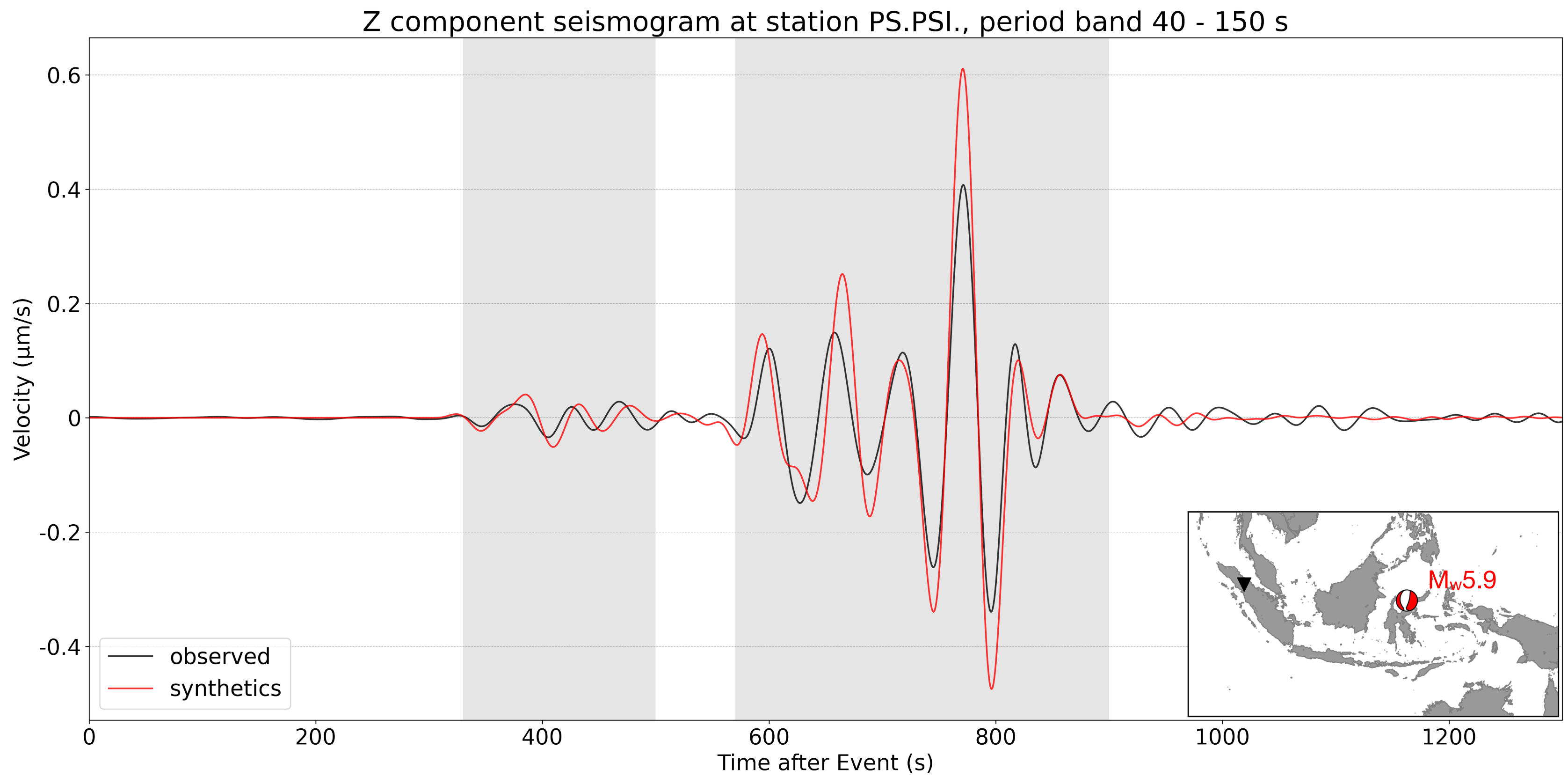

Misfit development

A **multi-scale approach** is adopted where long periods are inverted for first (Bunks et al., 1995)
[this mitigates the risk of entrapment in local minima and cycle skips]

As we go to shorter periods, we are able to **successively add more data**. This can be attributed to an improved waveform match and body wave signals becoming clearly identifiable
[this increase is indicated by the number of windows shown below]

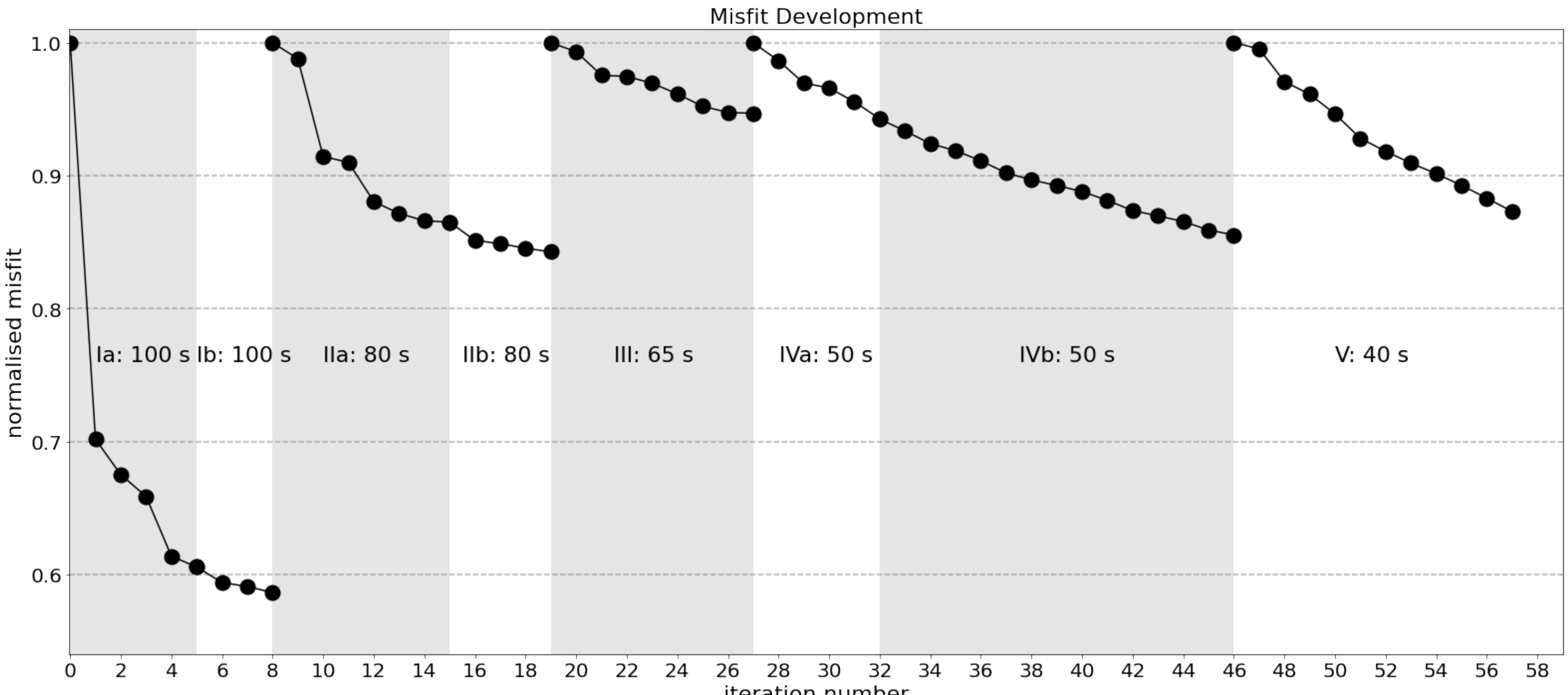

Minimum period	100 s	→	40 s
Number of windows	20,594	→	32,081

A more detailed technical overview can be found in the appendix

Waveform match improvement

The waveform match across all period bands shows **initial delays in observed waveforms**.

[note the insufficient waveform match at 65 s but the subsequent excellent misfit for the initial iteration at 40 s]

From 40 s onwards, two windows are selected: one around the (smaller-amplitude) body wave and one around the main surface wave arrival.

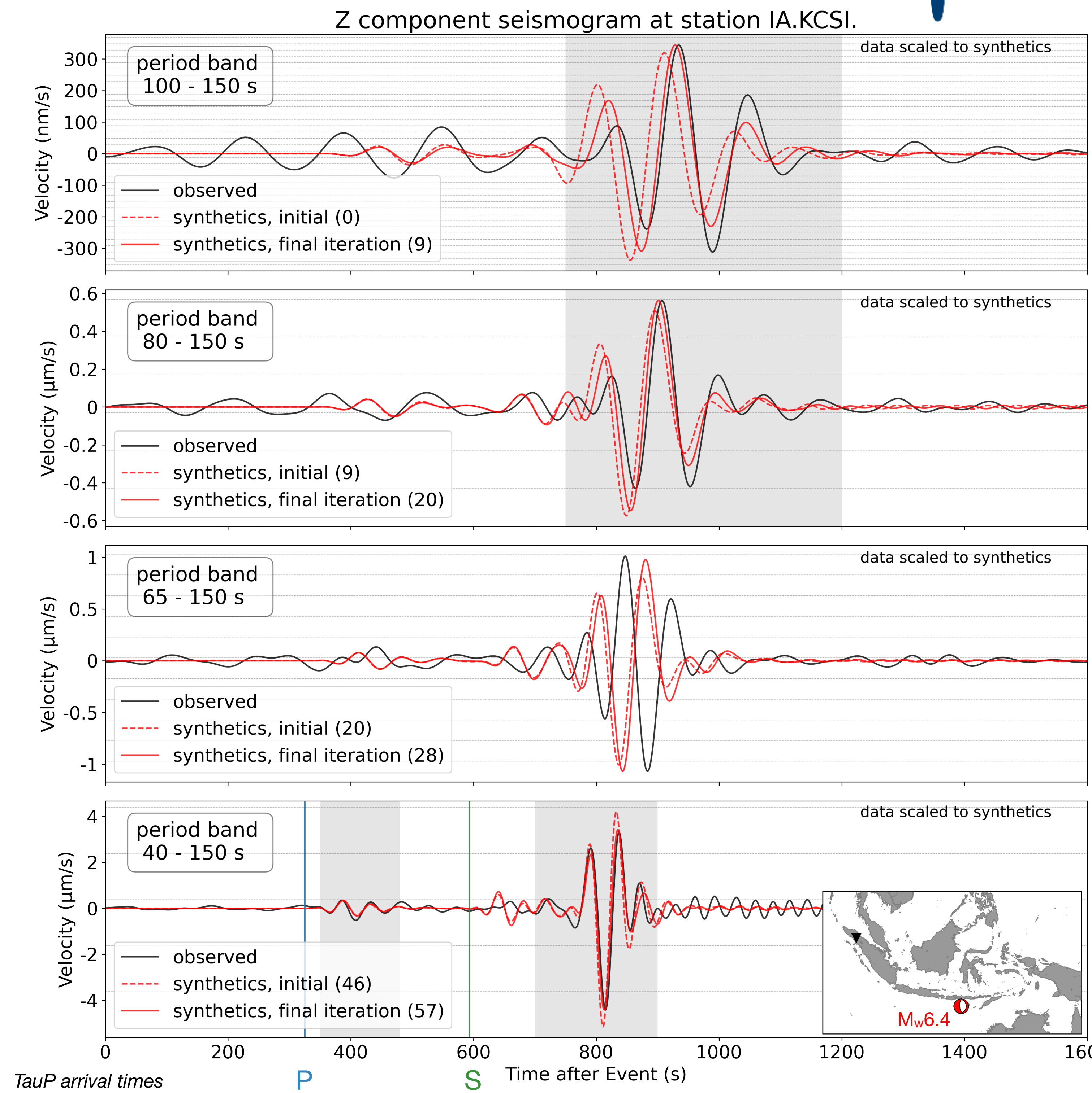

40 s model: Regional, shallow low-velocity zone

Initial model updates focus on including a **regional, shallow low-velocity zone**, the need for which is already apparent from the strong initial delays in observed waveforms.
[this is in well agreement with global models, e.g. *S40RTS,* Ritsema et al. (2011)]

We observe significantly **stronger anomaly amplitudes** compared to ray tomographic images, as is commonly observed in waveform tomographic studies (e.g. Fichtner et al., 2010). We observe the **strongest update in the S wave parameters** (> 12 %).
[at these long periods, the wavefield is dominated by surface waves which are most strongly sensitive to S wave structure]

100 km depth slice

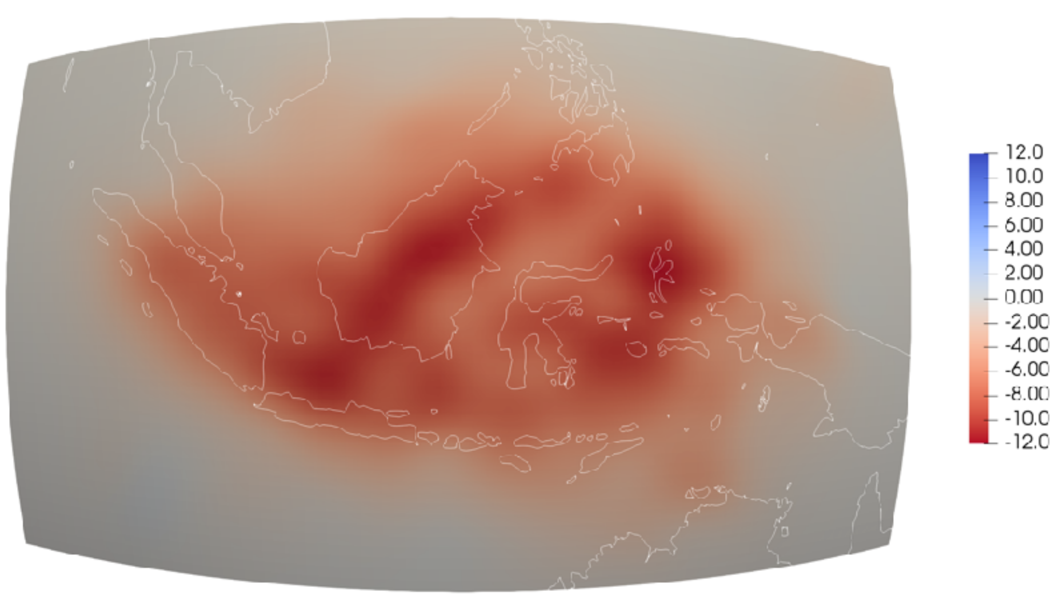

VSH

100 km depth slice

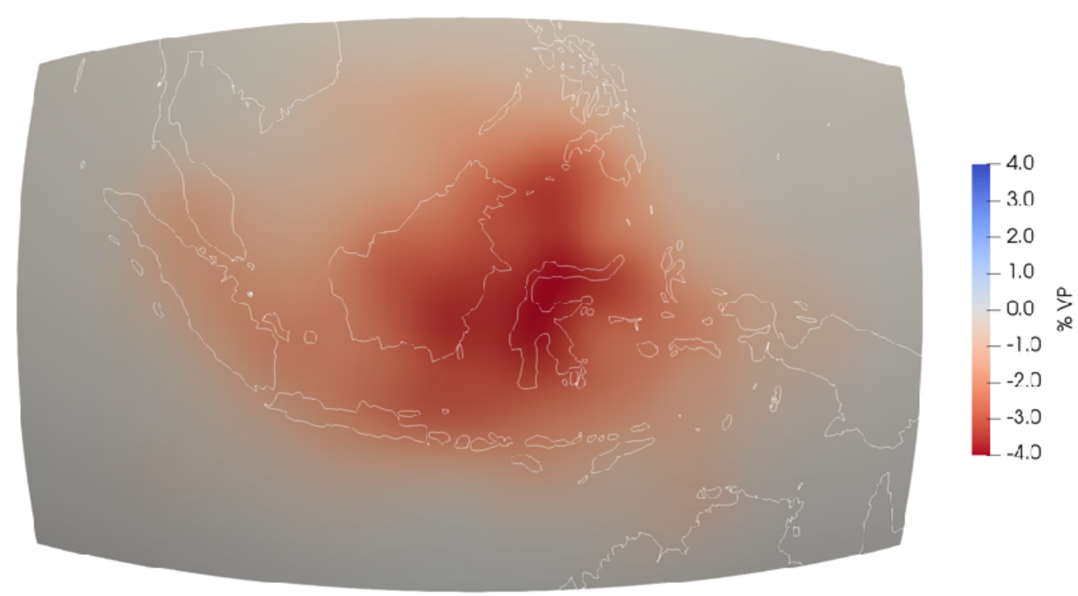

VP

The perturbations are relative to the initial model (*CSEM*, Fichtner et al. 2018)

40 s model: Sunda slab

The **Sunda slab** in the West is the most prominent feature of the current model and extends down to the **mantle transition zone** as shown below

From 50 s onwards, the 180° curvature of the Banda Arc in the East becomes apparent

We expect more details to appear as we add shorter period data in future simulations

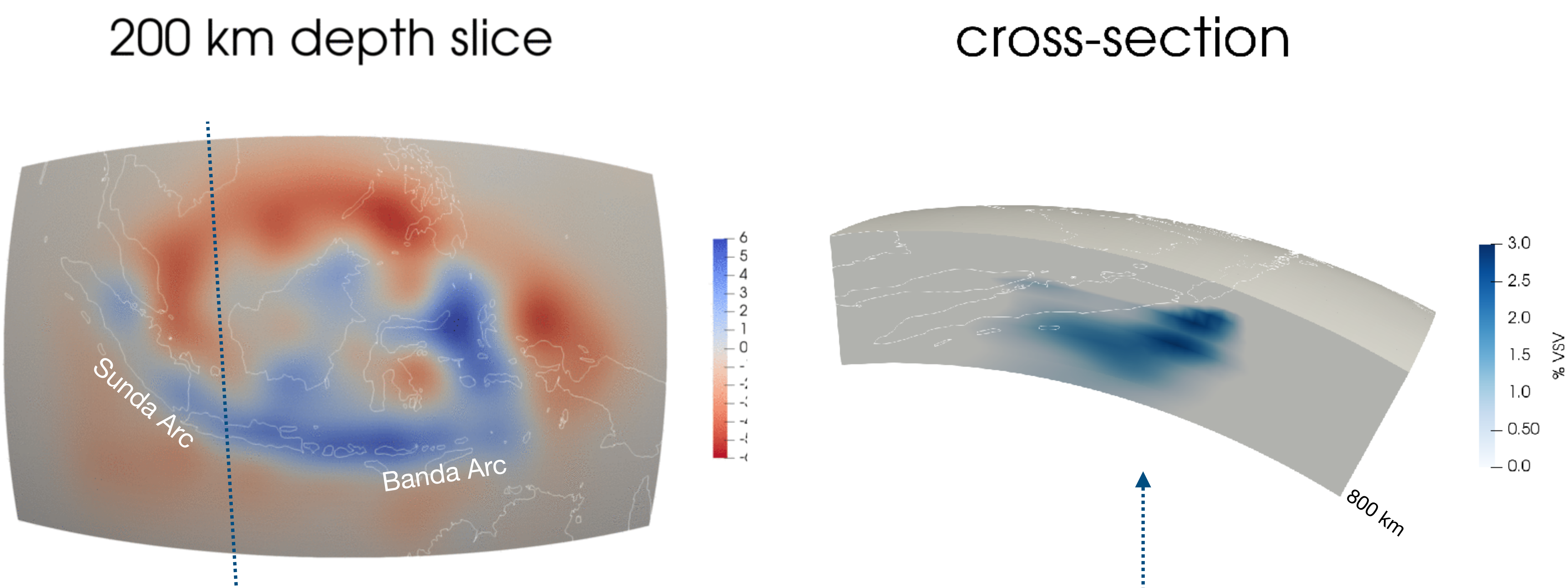

Conclusion and outlook

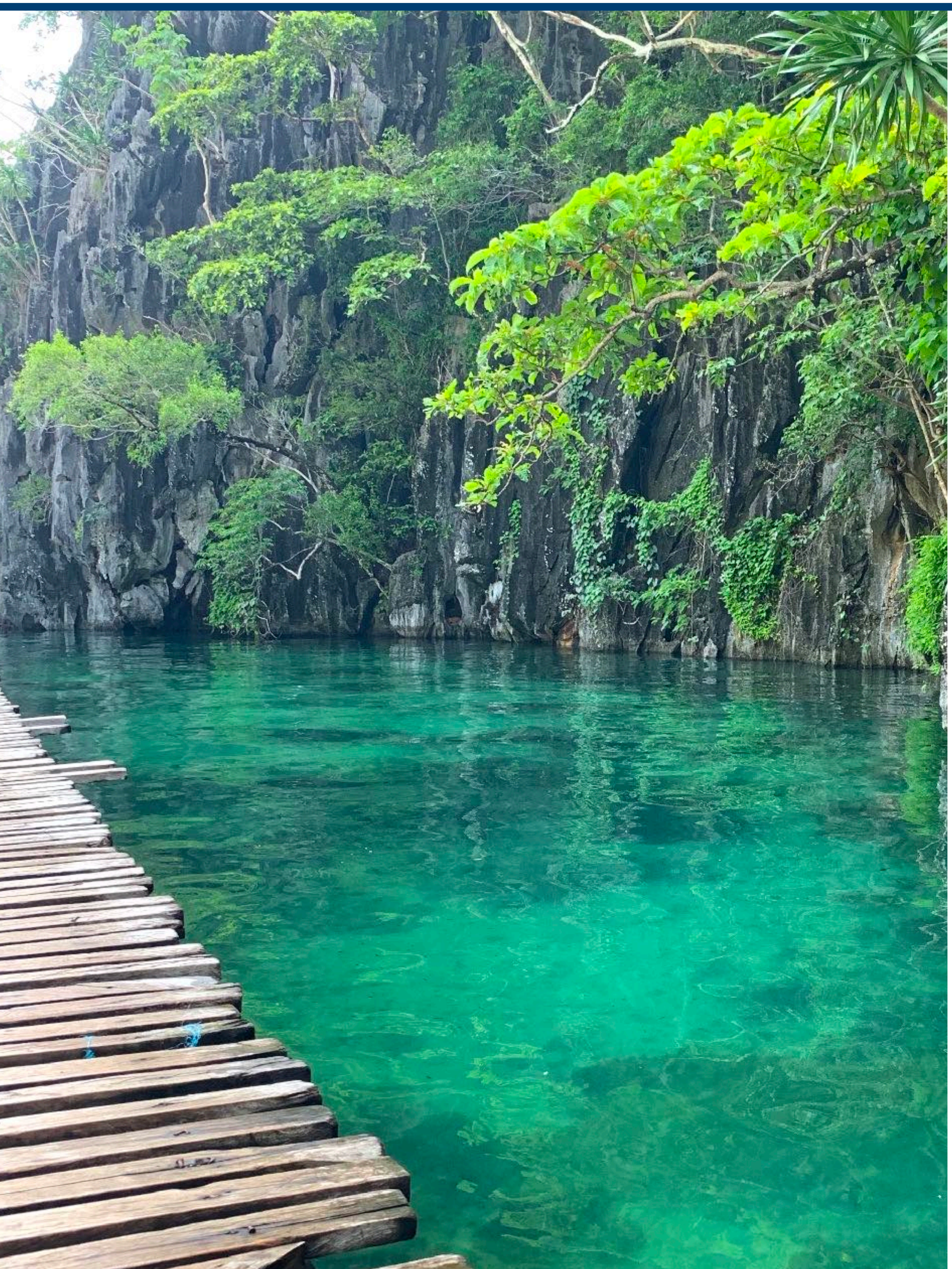

Palawan, Philippines

Conclusion

- We image v_{SH}, v_{SV}, v_P and density using adjoint waveform tomography at periods down to 40 s
- Our model resolves subsurface structures down to the mantle transition zone, including multiple subduction zones
- We observe strong heterogeneities > 12 %
  [strongest variations for v_{SH} parameter]

Outlook

- Continue inversion including shorter-period data: 30-150 s, 25-150 s, …
  [depending on data quality and model fit]

Questions?
Contact me via dwehner@esc.cam.ac.uk

References

Afanasiev, M., Boehm, C., van Driel, M, Krischer, L., Rietmann, M., May, D. A., Knepley, M. G., and Fichtner, A. (2019). “Modular and flexible spectral-element waveform modelling in two and three dimensions”

Bird, P., 2003. An updated digital model of plate boundaries. *Geochemistry, Geophysics, Geosystems*, *4*(3).

Bunks, Carey, et al. "Multiscale seismic waveform inversion." *Geophysics* 60.5 (1995): 1457-1473.

Dziewonski, A. M., & Anderson, D. L. (1981). Preliminary reference Earth model. *Physics of the earth and planetary interiors*, *25*(4), 297-356.

Ekström, G., Nettles, M., & Dziewoński, A. M. (2012). The global CMT project 2004–2010: Centroid-moment tensors for 13,017 earthquakes. *Physics of the Earth and Planetary Interiors*, *200*, 1-9.

Fichtner, A., Kennett, B. L., Igel, H., & Bunge, H. P. (2008). Theoretical background for continental-and global-scale full-waveform inversion in the time–frequency domain. *Geophysical Journal International*, *175*(2), 665-685.

Fichtner, A., van Herwaarden, D. P., Afanasiev, M., Simutė, S., Krischer, L., Çubuk-Sabuncu, Y., ... & Igel, H. (2018). The collaborative seismic earth model: generation 1. *Geophysical research letters*, *45*(9), 4007-4016.

Hall, R. (2012). Late Jurassic–Cenozoic reconstructions of the Indonesian region and the Indian Ocean. *Tectonophysics*, *570*, 1-41.

Maggi, A., Tape, C., Chen, M., Chao, D., & Tromp, J. (2009). An automated time-window selection algorithm for seismic tomography. *Geophysical Journal International*, *178*(1), 257-281.

Ritsema, J., Deuss, A. A., Van Heijst, H. J., & Woodhouse, J. H. (2011). S40RTS: a degree-40 shear-velocity model for the mantle from new Rayleigh wave dispersion, teleseismic traveltime and normal-mode splitting function measurements. *Geophysical Journal International*, *184*(3), 1223-1236.

Ruan, Y., Lei, W., Modrak, R., Örsvuran, R., Bozdağ, E., & Tromp, J. (2019). Balancing unevenly distributed data in seismic tomography: a global adjoint tomography example. *Geophysical Journal International*, *219*(2), 1225-1236.

Vallée, M., Charléty, J., Ferreira, A. M., Delouis, B., & Vergoz, J. (2011). SCARDEC: a new technique for the rapid determination of seismic moment magnitude, focal mechanism and source time functions for large earthquakes using body-wave deconvolution. *Geophysical Journal International*, *184*(1), 338-358.

van Herwaarden, D. P., Boehm, C., Afanasiev, M., Thrastarson, S., Krischer, L., Trampert, J., & Fichtner, A. (2020). Accelerated full-waveform inversion using dynamic mini-batches. *Geophysical Journal International*, *221*(2), 1427-1438.

Zenonos, A., De Siena, L., Widiyantoro, S., & Rawlinson, N. (2019). P and S wave travel time tomography of the SE Asia-Australia collision zone. *Physics of the Earth and Planetary Interiors*, *293*, 106267.

Langkawi, Malaysia

Technical details

Maximum period: 150 s

Gradient preconditioning:
1. Source imprint removal: Event kernels usually show large sensitivities around the source region. This source imprint has to be removed to avoid a strong localisation of model updates.
2. Smoothing: A diffusion-based smoothing is applied to the summed gradient.

The radius of the source imprint removal and the smoothing lengths for each period band can be found in the table on the next slide.

Inversion parameters:
- v_{SH}, v_{SV}, v_P and density
- a fixed attenuation model is used
- source parameters remain constant throughout the inversion

Optimisation scheme: Trust-region based L-BFGS (similar to van Herwaarden et al., 2020)

Technical details

Period band	Smoothing length (horizontal, vertical or in wavelengths)	Iterations	Number of events	Total windows	Unique source-receiver pairs	Source imprint removal (in km)	Mesh elements
100 s (Ia)	450 km 100 km	0 - 6	118	20,594	10,312	500	14,250
100 s (Ib)	375 km 100 km	6 - 9	118	20,594	10,312	500	14,250
80 s (IIa)	375 km 80 km	9 - 16	118	25,614	11,604	450	17,600
80 s (IIb)	300 km 80 km	16 - 20	118	25,614	11,604	450	17,600
65 s (III)	300 km 65 km	20 - 28	118	26,988	12,269	400	23,400
50 s (IVa)	depth-dependent smoothing [0.2, 1.0, 1.0]	28 - 32	117	25,583	12,060	350	33,866
50 s (IVb)	depth-dependent smoothing [0.2, 0.75, 0.75]	32 - 46	117	25,583	12,060	350	33,866
40 s (V)	depth-dependent smoothing [0.3, 0.5, 0.5]	46 - 57	106	32,081	12,960	300	49,680